ORGANIC PROCESS RESEARCH & DEVELOPMENT
OPR&D

香港科技大學圖書館
THE HONG KONG UNIVERSITY OF SCIENCE AND TECHNOLOGY UNIVERSITY LIBRARY

Subscriber access provided by Hong Kong University of Science and Technology Library

Full Paper

Palbociclib Commercial Manufacturing Process Development. Part I: Control of Regioselectivity in a Grignard-Mediated SNAr Coupling

Shengquan Duan, David Place, Hahdi H. Perfect, Nathan D. Ide, Mark Thomas Maloney, Karen Sutherland, Kristin E. Price Wiglesworth, Ke Wang, Mark A. Olivier, Fangming Kong, Kyle R Leeman, Jon Blunt, John Draper, Marie McAuliffe, Maria M O'Sullivan, and Denis Lynch

Org. Process Res. Dev., **Just Accepted Manuscript** • DOI: 10.1021/acs.oprd.6b00070 • Publication Date (Web): 12 May 2016

Downloaded from http://pubs.acs.org on May 13, 2016

Just Accepted

"Just Accepted" manuscripts have been peer-reviewed and accepted for publication. They are posted online prior to technical editing, formatting for publication and author proofing. The American Chemical Society provides "Just Accepted" as a free service to the research community to expedite the dissemination of scientific material as soon as possible after acceptance. "Just Accepted" manuscripts appear in full in PDF format accompanied by an HTML abstract. "Just Accepted" manuscripts have been fully peer reviewed, but should not be considered the official version of record. They are accessible to all readers and citable by the Digital Object Identifier (DOI®). "Just Accepted" is an optional service offered to authors. Therefore, the "Just Accepted" Web site may not include all articles that will be published in the journal. After a manuscript is technically edited and formatted, it will be removed from the "Just Accepted" Web site and published as an ASAP article. Note that technical editing may introduce minor changes to the manuscript text and/or graphics which could affect content, and all legal disclaimers and ethical guidelines that apply to the journal pertain. ACS cannot be held responsible for errors or consequences arising from the use of information contained in these "Just Accepted" manuscripts.

ACS Publications

Organic Process Research & Development is published by the American Chemical Society. 1155 Sixteenth Street N.W., Washington, DC 20036
Published by American Chemical Society. Copyright © American Chemical Society. However, no copyright claim is made to original U.S. Government works, or works produced by employees of any Commonwealth realm Crown government in the course of their duties.

Palbociclib Commercial Manufacturing Process Development. Part I: Control of Regioselectivity in a Grignard-Mediated S_NAr Coupling

Shengquan Duan,[a] David Place,[a] Hahdi H. Perfect,[a] Nathan D. Ide [a†],Mark Maloney,[a] Karen Sutherland, [a] Kristin E. Price Wiglesworth,[a] Ke Wang,[a] Mark Olivier, [a] Fangming Kong,[a] Kyle Leeman, [a] Jon Blunt, [b] John Draper, [b] Marie McAuliffe, [c] Maria O'Sullivan,[c] and Denis Lynch [c]*

[a] Chemical Research and Development and Analytical Research and Development, Pfizer Worldwide Research and Development, Eastern Point Road, Groton, CT 06340

[b] Chemical Research and Development, Pfizer Process Development Facility, Ramsgate Road, Sandwich, Kent, CT13 9NJ, UK

[c] Pfizer Global Supply, Ringaskiddy, Cork County, Ireland

Table of Contents Graphic

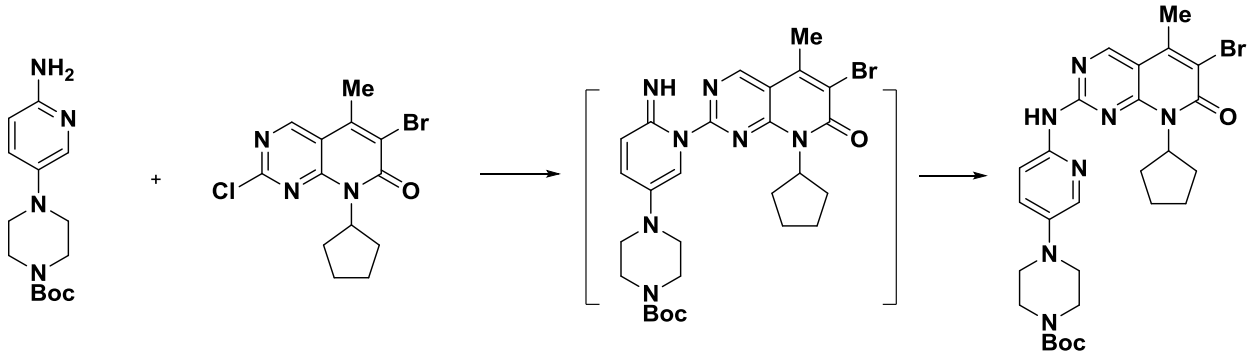

KEYWORDS: Palbociclib, S_NAr Coupling, Grignard, Regioselectivity

ABSTRACT: This is the first in a series of three papers describing commercial manufacturing process development for palbociclib (**1**). This manuscript focuses on the S_NAr coupling between aminopyridine **3** and chloropyrimidine **7**. The regioselectivity of the S_NAr coupling was studied from a synthetic and mechanistic perspective. Grignard bases were identified as the preferred class of bases for this reaction, allowing for a simplified process and reduced usage factor for aminopyridine **3**. The development of this S_NAr reaction into a scalable commercial manufacturing process is also described.

INTRODUCTION

Cyclin-dependent kinases 4 and 6 (CDK4/6) are key regulators of the cell cycle, involved in cellular progression from growth phase (G1) into the phase associated with DNA replication. [1a-d] Increased CDK 4/6 activity is frequently observed in estrogen receptor-positive (ER+) breast cancer (BC). [2a-d] Palbociclib (**1)** (Figure 1) is a highly selective, reversible inhibitor of CDK 4/6, intended to block tumor cell proliferation. Palbociclib received accelerated approval from the United States Food and Drug Administration (FDA) in February 2015. It is used in combination with letrozole for the treatment of postmenopausal women with estrogen receptor-positive, human epidermal growth factor receptor 2-negative (ER+/HER2-) advanced breast cancer as initial endocrine-based therapy. Palbociclib is marketed under the brand name IBRANCE®.

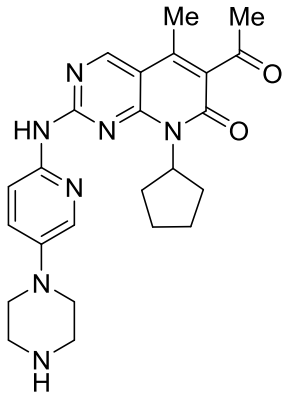

1

Figure 1. Structure of Palbociclib (1)

The evolution of the manufacturing process for palbociclib is shown in Schemes 1, 2, and 3. The discovery chemistry synthesis [3] of **6** (**1**-HCl salt) is shown in Scheme 1. While this route allowed for the preparation of preclinical supplies, it posed two major issues for further scale-up.

First, the coupling of **2** and **3** was problematic, with a yield at only 38%. Second, the Stille coupling required an expensive, toxic vinyl tin reagent.

Scheme 1. Discovery Route to Palbociclib

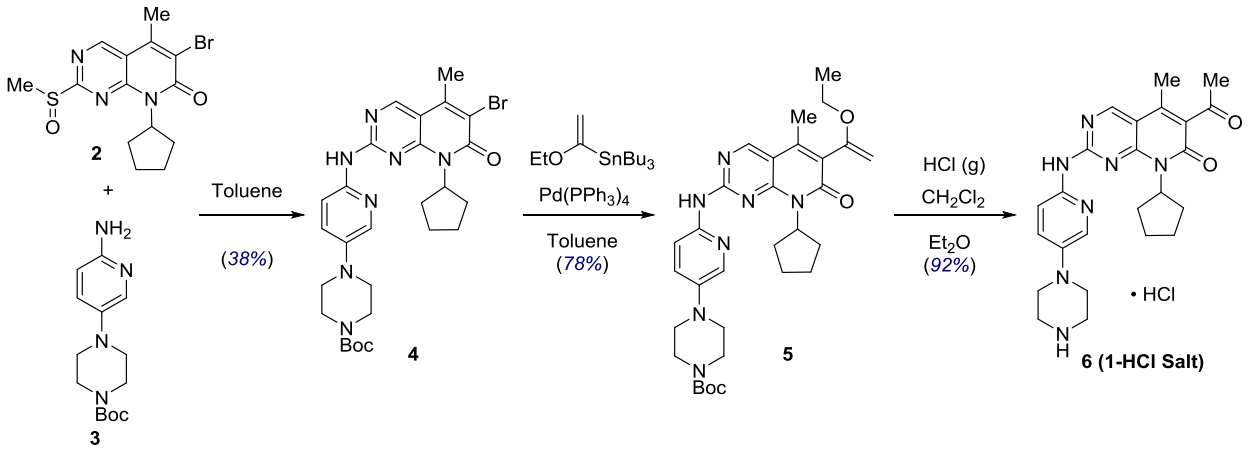

Nevertheless, the discovery chemistry route is highly convergent, and the last two steps had good chemical conversions. Thus, it became the basis for the initial process chemistry route (Scheme 2). The highlights of this route [4] include: (1) coupling of **3** and **7** using a strong base (LHMDS), which greatly improved the yield; (2) replacement of the Stille coupling with a Heck coupling, which eliminated the need for the vinyl tin reagent; (3) isolation of the API as an isethionate salt, with isethionic acid used to facilitate the hydrolysis of the enol ether and removal of the Boc protecting group. Although this early process chemistry route was amenable to scale-up, there were still a few aspects that were not ideal for commercial manufacturing. First, more than two equivalents of **3** were required for good yield in the S_NAr coupling. Second, lack of regioselectivity [5] in the Heck reaction resulted in challenges for impurity control. Finally, the physical properties of the isethionate salt were not suitable for drug product manufacturing, which resulted in a final form change to the API free base.

Scheme 2. Clinical Manufacturing Route to Palbociclib

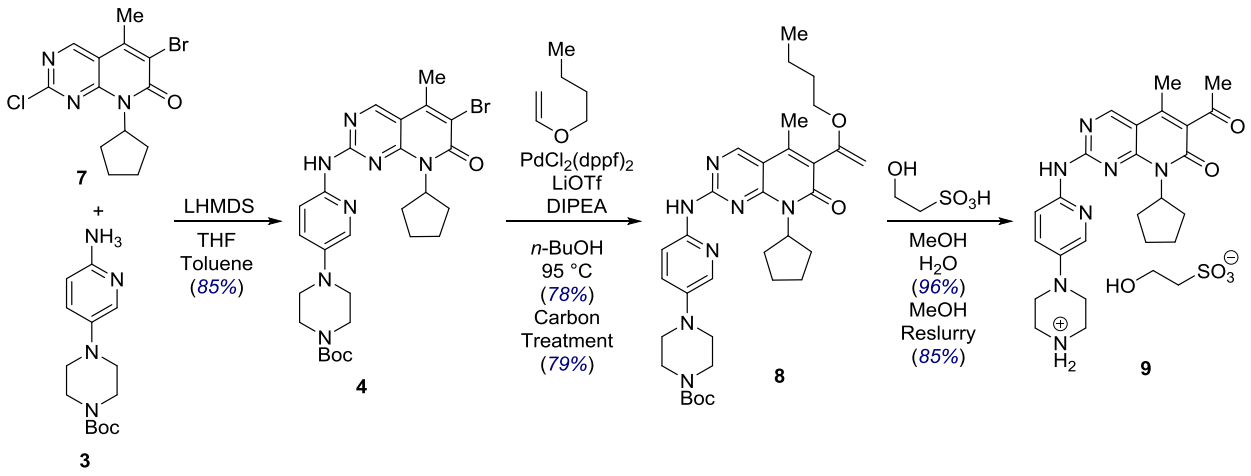

During commercial route development, a variety of new synthetic routes [6] were evaluated. These approaches include modification of step order of the enabling synthesis, synthesis of the penultimate by palladium-catalyzed amination [7], construction of the pyridinone ring through Friedländer annulation [8], Larock annulation reaction [9], and Knorr cyclization [10]. However, none of these approaches were cost effective compared to the enabling route, so the decision was made to further develop the enabling route for commercial use. A thorough process development program was carried out to improve the scalability, efficiency, and quality of the enabling process. The final proposed commercial manufacturing process for palbociclib is illustrated in Scheme 3.

Scheme 3. Commercial Manufacturing Process for Palbocicilib

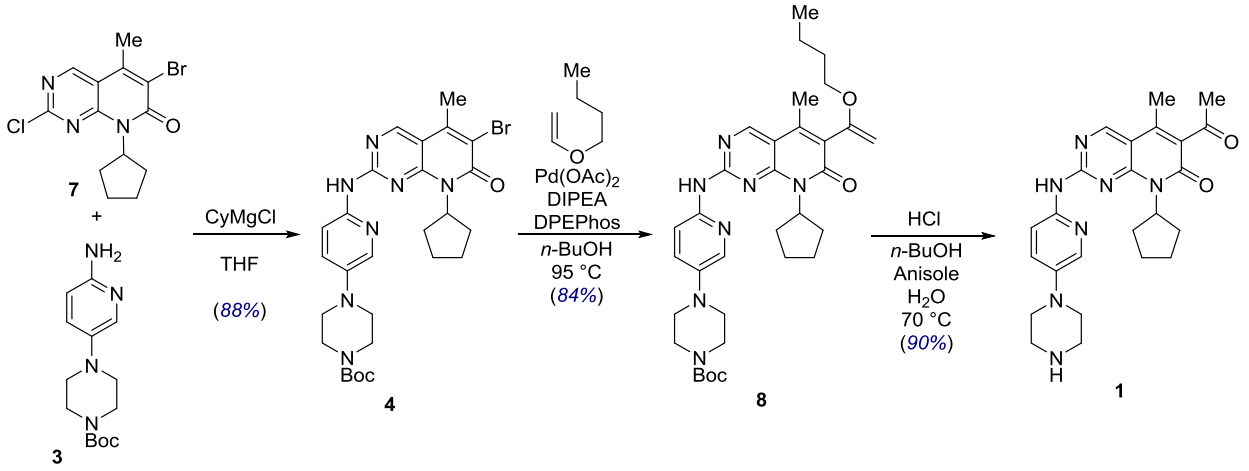

Herein we publish a series of three papers that document our journey to develop the commercial manufacturing process for palbociclib. This paper (Part I) focuses on the development of the Grignard-mediated S_NAr coupling between compound **3** and compound 7. Part II [11] describes the installation of the enol ether side-chain by Heck coupling. Part III [12] describes the final deprotection step and the API particle engineering efforts.

RESULTS AND DISCUSSION

The nucleophilic aromatic substitution (S_NAr) reaction between the amino pyridine compound **3** and the pyrimidine compound (**2, 10, 7**) is shown in Scheme 4. This reaction looks fairly straightforward, but it involves a relatively complicated mechanism. Extensive development work was completed in order to identify suitable conditions for this coupling, and to optimize the conditions for process robustness.

Scheme 4. S_NAr Coupling Reaction

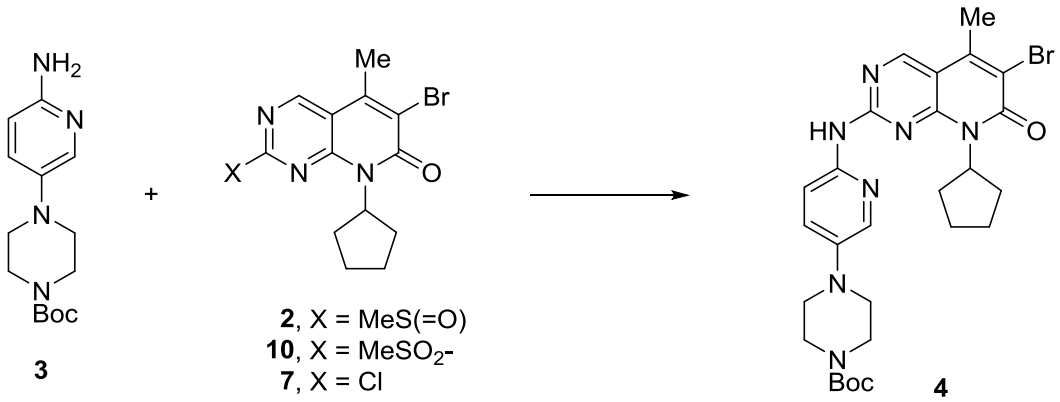

Selection of the Pyrimidine Coupling Partner

Different leaving groups (X, Scheme 4) were evaluated for the pyrimidine component. For the preparation of the first clinical supplies, the sulfoxide compound **2** was used. A variety of reaction conditions had been examined, and the best yield (38%) was obtained [13] when the two compounds were reacted in refluxing toluene. Change of solvents and reaction temperature did not improve the yield. Fortunately, the product **4** precipitated directly from the reaction mixture with acceptable purity. Change of the leaving group to sulfone [14a-c] (compound **10**) improved the reactivity, but only marginally improved the yield to 50%. Besides the low yield encountered in the coupling with **2/10**, the syntheses of **2/10** were lengthy, requiring 10 and 11 linear steps respectively. [15] To overcome the difficulty to access these compounds, an analogous compound **7** was identified. Synthesis of **7** is much more efficient, as it is accessible in four steps from commercially available dichlorobromopyrimidine **11** [16] (Scheme 5). Thus, **7** was selected as starting material for palbociclib synthesis and the subsequent development has been focused on coupling between **3** and **7**.

Scheme 5. Synthesis of 7

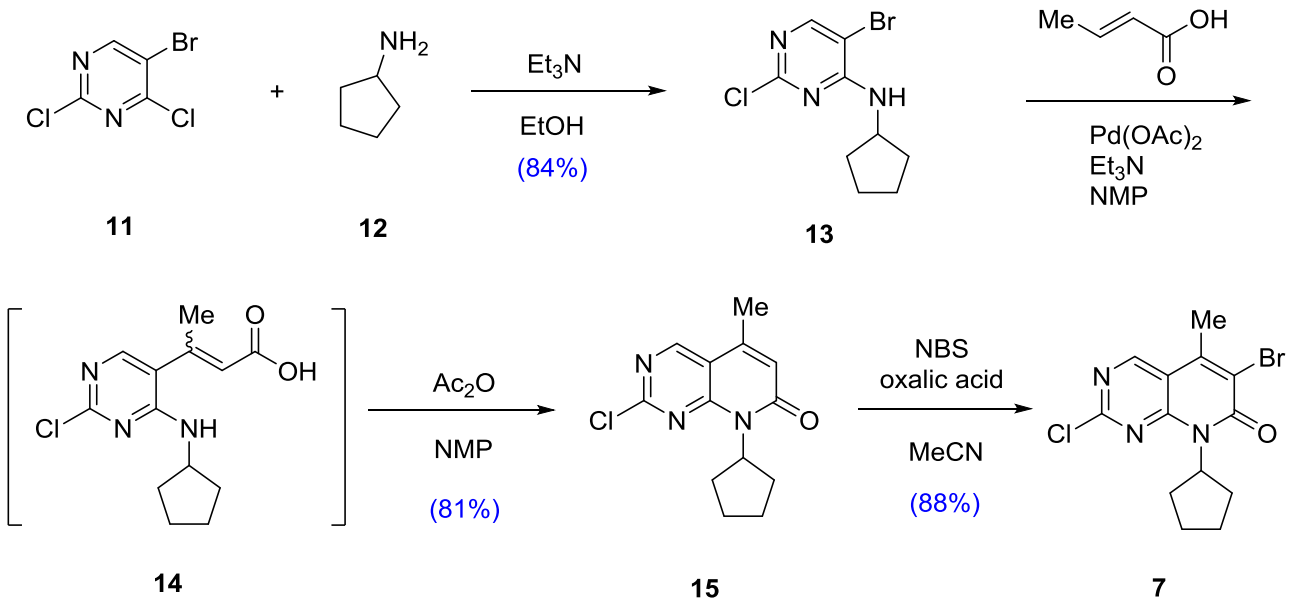

Alternative Approaches for Coupling of 3 and 7

To address the issues encountered in the enabling synthesis, many alternative approaches for the coupling between **3** and **7** were investigated. These conditions include: palladium catalyzed coupling, S_NAr coupling under neutral conditions, acidic conditions, and weak basic conditions, and fluoride catalyzed coupling. While all these conditions failed to meet our requirements, studies on these reactions provided insight on the reaction mechanism and helped us identify the optimal reaction conditions using strong base.

1. Palladium Catalyzed C-N Coupling

Palladium catalyzed C-N cross coupling had been investigated to couple **3** with **7** following literature procedures. [17a-b] A few catalysts ($Pd(OAc)_2$, $Pd_2(dba)_3$, and POPd), ligands (BINAP, DavePhos, and JohnPhos), bases (NaO*t*-Bu, K_3PO_4, and Cs_2CO_3), and solvents (toluene, DME) were screened (Figure 2.). While most of these reactions gave very low yield of the desired product, the palladium phosphinous acid catalyst (POPd) provided the best yield (40%). Further optimization of reaction conditions focusing on POPd catalyst failed to improve this yield. This

coupling method was deemed to be impracticable considering the cost associated with the catalyst and the modest yield.

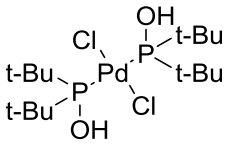

POPd

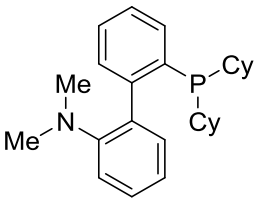

DavePhos

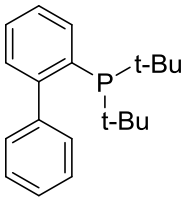

JohnPhos

Figure 2. Structure of POPd, DavePhos and JohnPhos

2. S_NAr Coupling of 3 and 7 under Neutral and Acidic Conditions

In the course of our investigation of alternate conditions for this S_NAr coupling, we also evaluated the reactivity under neutral conditions. Coupling of **3** with **2/10** required heating because of the weak nucleophilicity of the amino pyridine. Compared to the sulfone and sulfoxide compounds, the chloride compound **7** is less reactive, which makes this transformation even more challenging. In fact, no desired product was observed when **3** was combined with **7** under neutral conditions, even in refluxing toluene. The ambident reactivity of **3** turned out to be the biggest challenge for this coupling. Aminopyridine **3** is an ambident nucleophile [18] that can react at either the 2-amino group or the pyridine ring nitrogen. In fact, the undesired regioisomer **16** was dominant under neutral conditions, suggesting that the pyridine nitrogen was more nucleophilic (Scheme 6).

Scheme 6. Regioselectivity Issue in Coupling of 3 and 7

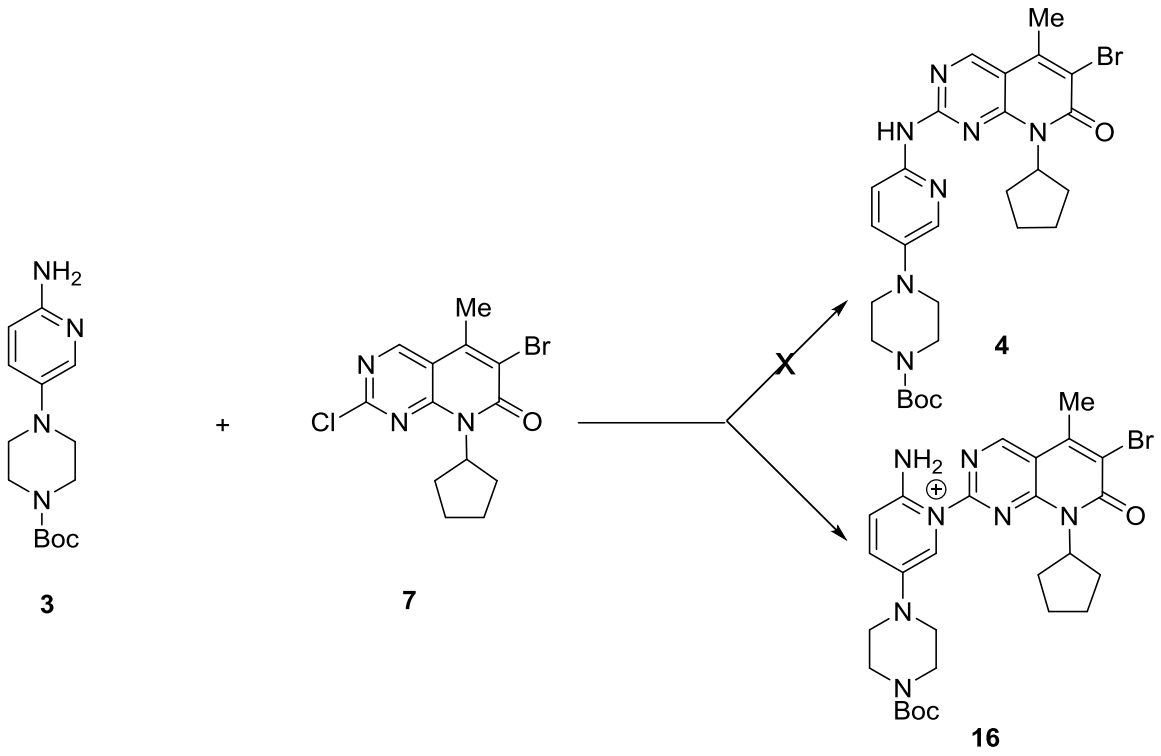

Acid catalysis was first explored to re-direct the selectivity [19]. It was envisioned that the amino-nitrogen would be available for nucleophilic substitution after the more basic pyridine nitrogen was blocked by forming a pyridinum salt with acid (the calculated pKa of the conjugated acid for the pyridine nitrogen and amino nitrogen was 8.2 and 3.1 respectively). To that end, a few hydrochloride salts of **3**, with varied amount of counter-ion (1.0 equiv. 2.0 equiv. and 3.0 equiv.), were prepared, and subjected to the coupling with **7**. It turned out that this approach did not alter the coupling pathway at all. While the reaction proceeded very slowly, the pyridinum salt **16** was obtained without exception in all of the experiments.

3. S_NAr Coupling of 3 and 7 under Weak Basic Conditions

The problematic ambident reactivity was also observed when weak bases were used to assist the reaction. Table 1 listed the results of a few coupling experiments under weakly basic conditions. As can be seen from this table, none of the organic bases resulted in desired product, although some of them did react with **7**. When pyridine, Hunig's base, and N-methylmorphline were used

(entry 1), the reaction proceeded slowly to give the pyridinum side product **16**. This outcome is similar to when the reaction was run under neutral or acidic conditions. For the more nucleophilic bases, such as DMAP, imidazole, and DABCO [20] (entries 2, 3, 4), the bases reacted with **7** but the resulting compounds did not serve as a reactive intermediate. In the reactions with DMAP and imidazole, the intermediates were stable and no further reaction with **3** was observed. In the case of the DABCO reaction, the liberated chloride from the substitution reaction attacked and opened the DABCO ring. None of these results with weak organic bases were considered to warrant any additional investigation. The inorganic bases gave similar results (Entry 5). When carbonates (K and Cs) were used, the pyridinum product **16** was again obtained.

Table 1. Results of S_NAr Coupling under Weak Basic Conditions

Entry	Base	Desired Product Yield	Major Side Product
1	Pyridine, Hunig's base, N-methylmorphline	<5%	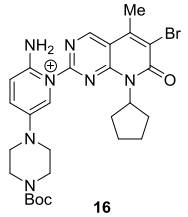 **16**
2	DMAP	<5%	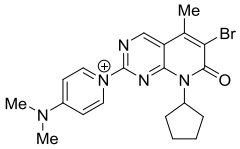 **17**
3	Imidazole	<5%	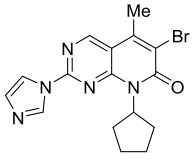 **18**
4	DABCO	<5%	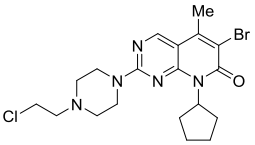 **19**

5	K_2CO_3, Cs_2CO_3	<5%	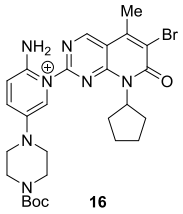 16

4. S_NAr Coupling of 3 and 7 under Fluoride Catalyzed Conditions

Fluoride-catalyzed amination was also investigated based on literature reports suggesting that fluoride catalysis might be effective for this type of reaction. [21] The accepted mechanism for this type of reaction is that the chloride electrophile is converted to the corresponding fluoride analog, followed by reaction with the nucleophile. However, when compound **3** and **7** were heated with CsF and KF in presence of crown ethers (18-C-6 or 15-C-5 respectively), a complicated mixture was obtained in both reactions with only small quantity of desired product. The conditions identified by Senanayake et al [22] in a similar S_NAr coupling were also investigated. In that study, the monomethylpolyglyme solvent (TGME) played a critical role to activate the CsF by coordinating with Cs^+ and hydrogen bonding to the naked fluoride ion. However, this reaction failed to give any desired product in our case. The major product isolated from this reaction was identified as the displacement product in which the chloride was displaced by the TGME solvent (Compound **20**, Figure 3). This suggested that the amino pyridine compound was less nucleophilic than the alcohol under fluoride catalysis conditions.

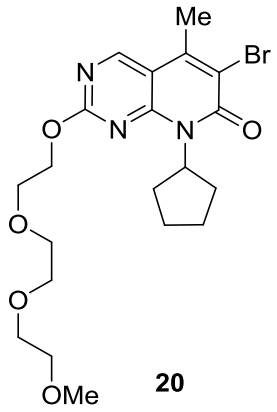

20

Figure 3. Product Formed under Fluoride Catalyzed Reaction

S_NAr Coupling under Strong Basic Conditions

The HOMO calculation of compound **3** at neutral state indicated that the nucleophilicity of the pyridine nitrogen and the amino nitrogen was comparable (Figure 4). This explained why the reaction with **3** showed ambident reactivity. Formation of the undesired regioisomer (**16**) in most cases further suggested that the nucleophilic reaction with the pyridine nitrogen was kinetically favored. When the similar calculation was done on the deprotonated **3**, it showed that the nucleophilicity can be differentiated between these two nitrogens, with the exocyclic nitrogen bearing much higher electron density. Considering that this would lead to the desired regioselectivity, we turned our attention to coupling with strong bases.

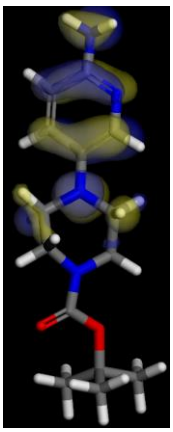

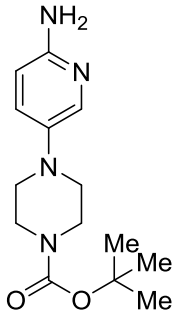

3

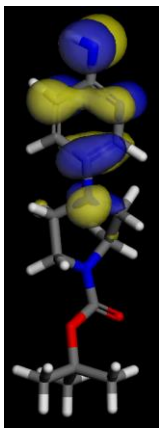

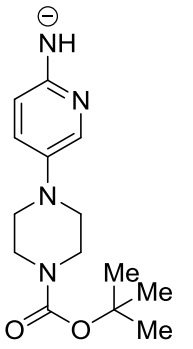

Deprotonated 3

Figure 4. HOMO Calculation of 3 and Deprotonated 3

1. S_NAr Coupling: LiHMDS Base

LiHMDS was found during early process development work to produce the desired coupling product in good yield. When **3** was treated with LiHMDS, the lithiated amide reacted readily with **7**, at ambient temperature, to give the desired product. However, a new problem was introduced with the use of strong base because the product is significantly more acidic than the starting material. When less than 2 equivalents of LHMDS were used, the reaction stalled at <50% conversion (Table 2, entry 1). Simply adding a second equivalent of LiHMDS (Table 2, entry 2) resulted in higher conversion (starting material consumption) but not higher yield since the starting material and the product were not stable to excess LiHMDS (*vide infra*). The reaction worked the best when 2+ equivalents of aminopyridine **3** and 2+ equivalents of LHMDS were used at the same time (Table 2, entry 3).

Table 2. S_NAr Coupling with LiHMDS as Base

Entry	Stoichiometry of LiHMDS	Stoichiometry of 3	Yield
1	1.5	1.6	27.6%
2	2.5	1.6	53.7%
3	2.5	2.2	85%

While the conditions in entry 3 were effective and were used to produce material for clinical supplies, the requirement for 2+ equivalents of aminopyridine **3**, an advanced intermediate, was not ideal. Additional investigations into stoichoimetry and addition modes did not reveal any additional improvements. Investigations also showed that NaHMDS and KHMDS were inferior to LiHMDS, providing a more complex purity profile. In order to reduce the usage factor of the advanced intermediate **3**, mechanistic work was carried out to understand why the second

equivalent of **3** was necessary. Two on-line analytical tools were utilized to collect the required information. First, in-situ ReactIR monitoring of the reaction progress provided some insight into the reaction mechanism (Figure 5). Based on the IR data, deprotonation of aminopyridine **3** was instantaneous upon addition of LiHMDS. Subsequent addition of 7 resulted in the formation of a small amount of desired product **4** and a larger amount of an intermediate that slowly converted to desired product **4**. Using a Mettler Toledo Easy Sampler® probe, a tool that can take multiple samples in short period, we were able to capture samples containing this intermediate. Structure elucidation, performed on samples that had undergone an aqueous quench, confirmed that the isolated intermediate was the pyridinum salt **16**. It is believed that the actual intermediate under strong basic conditions bears the imino form **21**, which converts to the protonated form **16** upon quenching.

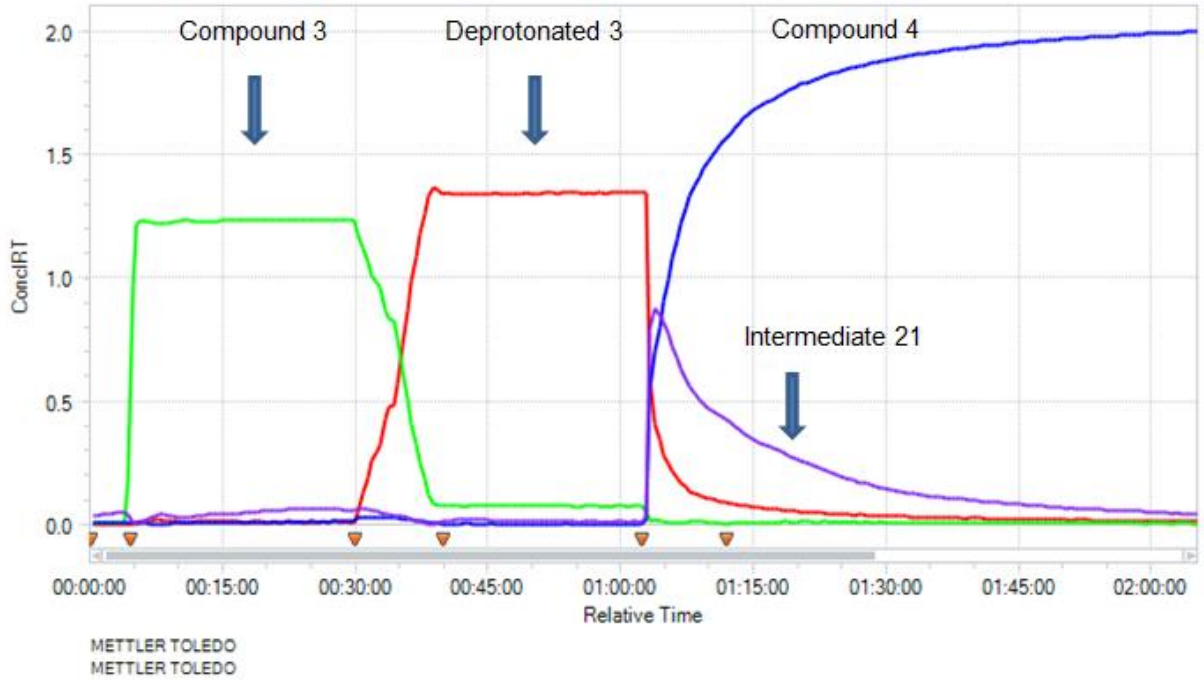

Figure 5. ReactIR Monitoring of the LiHMDS Reaction

Scheme 7. Reaction Intermediate before and after Aqueous Quench

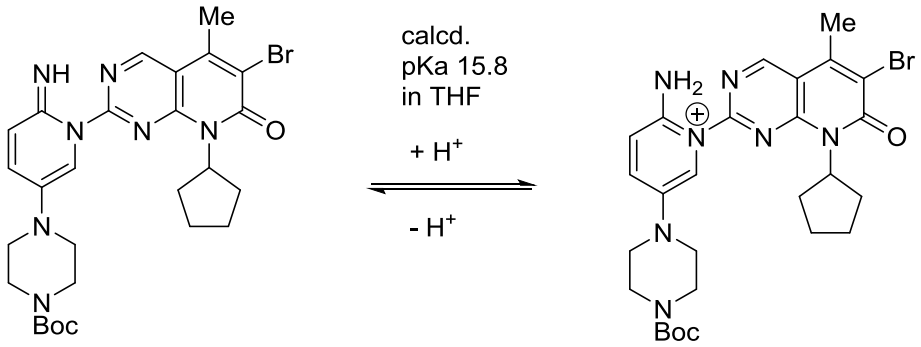

21 **16**

The discovery of this intermediate suggested that while the electron density on the amino nitrogen increased after deprotonation by strong base, the reaction between the pyridinyl nitrogen and **7** was still kinetically favored. This also suggested that the coupling between **3** and **7** was not a simple S_NAr displacement, but involved a more complicated mechanism.

We initially consider a bimolecular mechanism that involved reaction of **21** with a second equivalent of deprotonated **3** (Scheme 8). In this mechanism, the imino-intermediate **21** would first be formed in the reaction then a second equivalent of lithiated **3** would react with the imino intermediate in another S_NAr reaction, liberating the excess **3** and generating the desired product.

Scheme 8. Initially Proposed Reaction Mechanism between 3 and 7

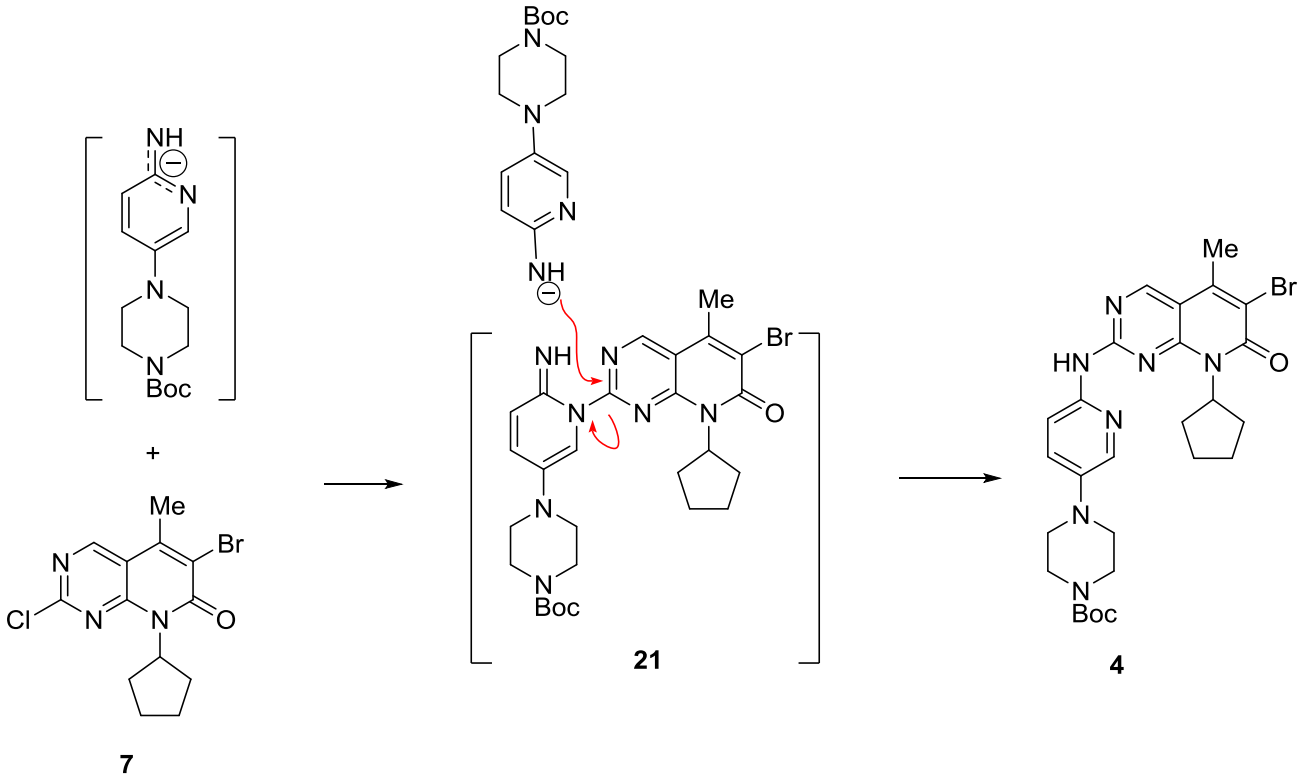

This mechanism would explain why the second equivalent of **3** was required in the coupling reaction. However, when the reaction conversion data was modeled using kinetics modeling software DynoChem®, it was found that the proposed 2nd order reaction mechanism did not fit the data. Instead, the data fitting supported a model of 1st order reaction for the conversion of **21** to **4** (Figure 6).

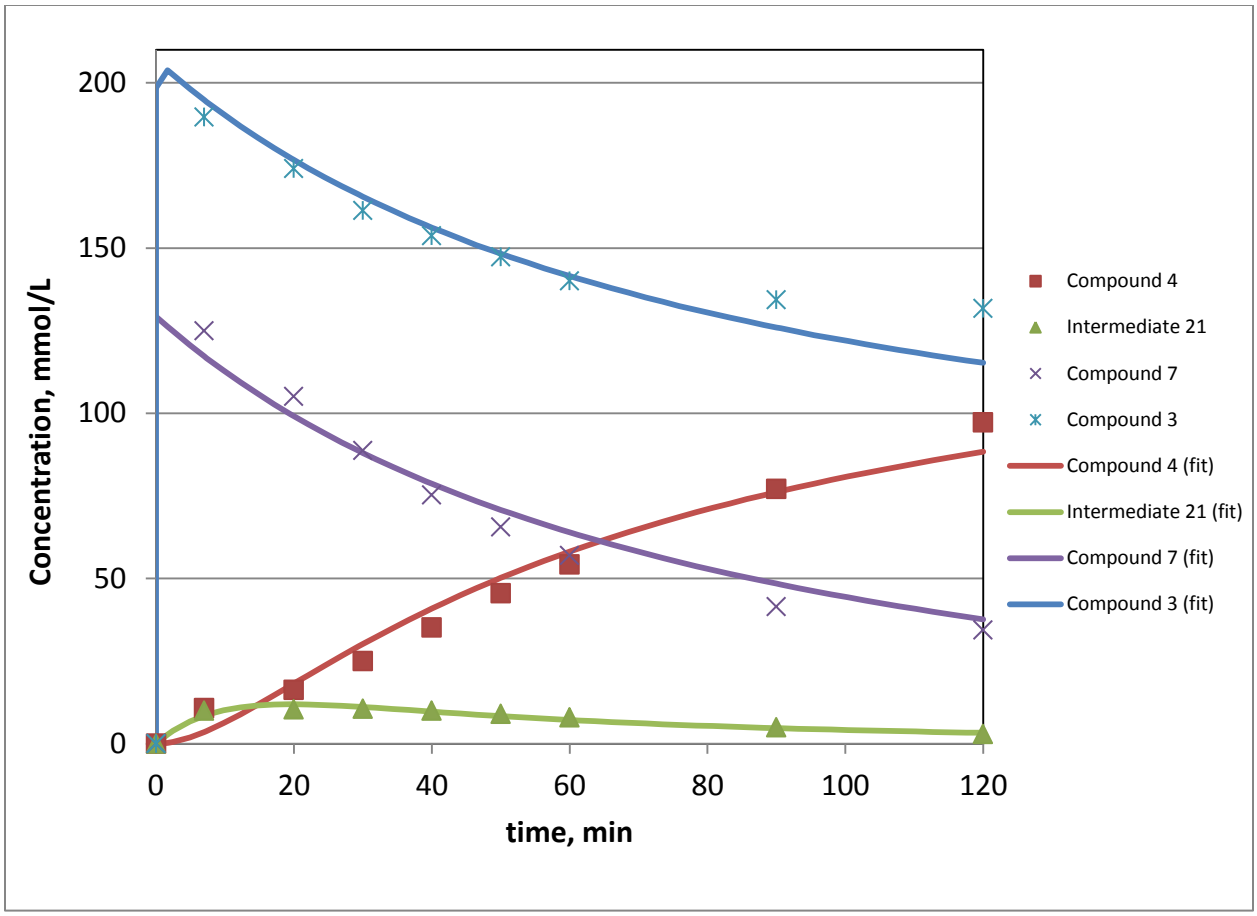

Figure 6. DynoChem Modeling of LiHMDS Reaction

To further confirm the 1st order reaction mechanism, a series of experiments at -20 °C, 0 °C, and 20 °C were performed and the in-situ IR data were exported to the iC Kinetics™ software for kinetic modeling. The kinetic simulation confirmed that the decay of **21** was indeed first order, and the 2nd equiv. of lithiated **3** did not participate in the rate determining step (Figure 7).

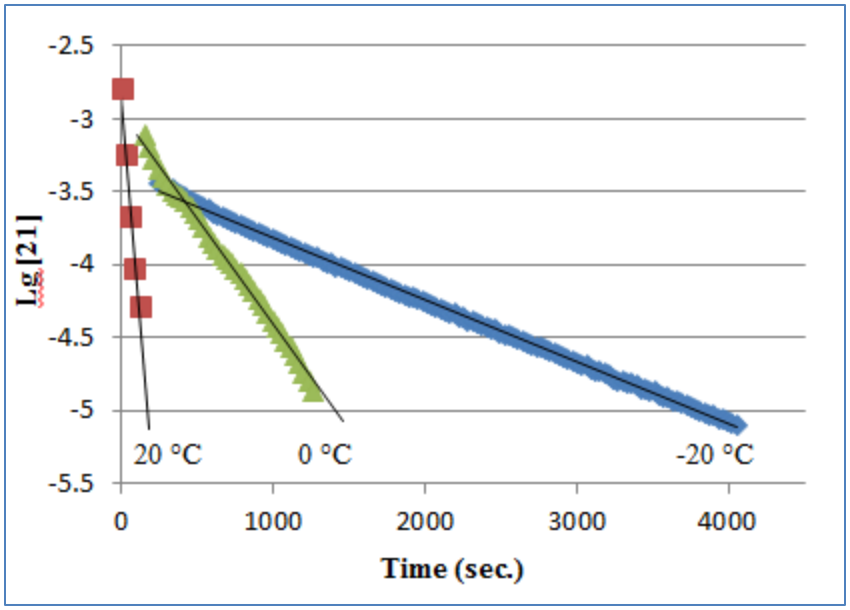

Figure 7. Kinetics Study at Different Temperatures

The above studies suggested that the conversion of the imino intermediate **21** to the desired product was through an intramolecular rearrangement process. Multiple mechanistic pathways are possible, but based on the work of Chapman [23a-c] and Granik [24], we suspect that the reaction mechanism is a [1,3] aryl shift via a four-membered ring transition state (Scheme 9).

Scheme 9. Rearrangement Mechanism

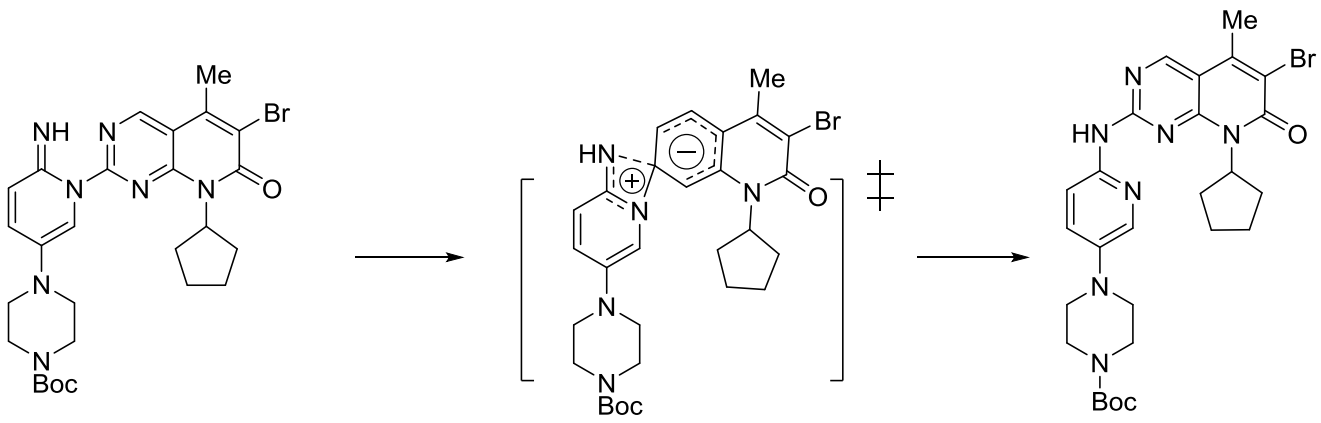

While the newly proposed mechanism fits better with the kinetics, it could not explain why the second equivalent of **3** was required to promote the yield (and not simply a second equivalent of LiHMDS). Careful study on the reaction profile identified one major impurity in the LiHMDS reaction mixture. This impurity has a molecular weight of 1174. Isolation and structure elucidation identified this impurity as a dimer of two product molecules (Compound **22**, Figure 8). The structure of this impurity suggested that the methyl proton was deprotonated under strong basic conditions and then underwent a possible 1, 6-addition to another product molecule. Exposure of product **4** to LiHMDS indeed reproduced the formation of this dimer. Similar degradation pathways were observed upon exposure of the chloropyrimidine 7 to LiHMDS.

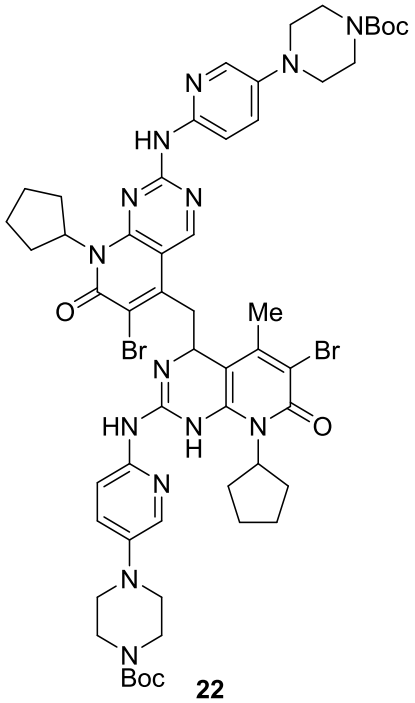

22

Figure 8. Structure of Dimer Impurity 22

The above observation explained the function of the second equivalent of **3**. It served as a buffer to consume the second equivalent of LiHMDS. The lithiated **3** was basic enough to deprotonate the acidic proton in the product, which drove the reaction to completion, but it was not strong

enough to abstract the proton in the methyl group, which was the root cause of the dimer formation. Without the second equivalent of LiHMDS, the reaction would stall. Without the second equivalent of **3**, the excess LiHMDS would react with the product and/or **7**, which resulted in impurity formation and low yield.

2. S_NAr Coupling: Grignard Base

On the basis of the mechanistic understanding, we decided to investigate a few other strong bases, attempting to find a strong base that does not promote the dimer (**22**) formation. While LiH and NaH failed to deprotonate **3**, tertiary alkoxide bases gave some interesting results. Based solely on pKa value, it was not expected that the alkoxide base would be able to deprotonate **3**. However, a complete consumption of **7** was indeed observed when NaO*t*-Bu, KO*t*-Bu, and NaO*t*-Am (2 equiv. of base with 1 equiv. of **3**) were tested. The yields of these reactions were disappointedly low at 30-40% though. The major impurity was due to reaction of water with **7** to give hydroxypyrimidine (**23**, Figure 9). When rigorous drying was applied on the starting materials and solvents, and the reaction was handled completely in the glove box, this impurity was minimized and up to 87% isolated yield was obtained with 2 equivalents of NaOt-Bu and 1.3 equivalents of **3**. However, such rigorous exclusion of water was obviously not practical at manufacturing scale. Note that impurity **23** was not observed in the LiHMDS reaction. It is believed that the major reaction pathway in the alkoxide reaction was slow, which provided the opportunity for the adventitious water to compete.

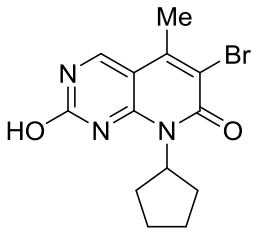

23

Figure 9. Structure of Hydroxypyrimidine 23

Another type of base that showed promise was the Grignard base. Reaction with *i*-PrMgCl (2 equiv. base and 2 equiv. **3**), gave comparable yield as the LiHMDS reaction. The reaction profile was cleaner with no dimer impurity detected. A test reaction, with the use of only 1.1 equiv. of **3** and addition of 2 equiv. of *i*-PrMgCl in two portions, led to the first successful reaction in which the usage factor of **3** was reduced to nearly 1. The initial 81% isolated yield was enhanced to 94% when optimal stoichiometry was identified: 1.3 equiv. of **3** and 2.2 equiv. of *i*-PrMgCl.

We initially suspected that the improved reaction profile might be due to increased stability of the product **4** in the presence of the Grignard base vs. LiHMDS, but the follow-up experiments showed that this was not the case. While exposure of product to *i*-PrMgCl did not generate the dimer impurity, it resulted in the rapid formation of des-bromo impurity **24** (Figure 10) via metal-halogen exchange reaction. Interestingly, this side reaction between **4** and *i*-PrMgCl was kinetically faster than the side reaction between **4** and LiHMDS.

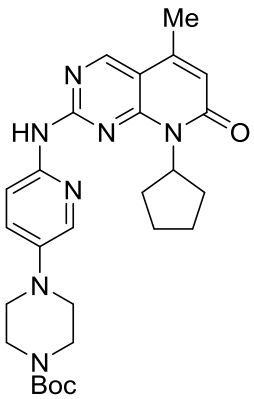

24

Figure 10. Structure of Des-Br Impurity 24

Kinetic study of the *i*-PrMgCl reaction was carried out to understand the difference from the LiHMDS reaction. Interestingly, the imino intermediate **21** was not detected by ReactIR in the Grignard reaction. Off-line analysis indicated very low level of this compound throughout the process. There are two possible scenarios: (1) the reaction mechanism completely changed and the reaction went through a direct S_NAr displacement or (2) the reaction mechanism was the same but the conversion of intermediate **21** to desired product was so fast that the concentration of the intermediate was always low and below the ReactIR detection limit. There is no solid evidence to prove one way or another. Either way, it can be concluded that the kinetics in the *i*-PrMgCl reaction were much faster than the LiHMDS reaction. As seen in Figure 11, the reaction went to completion at the moment the Grignard dosing was completed. Because of the fast kinetics of the main reaction, the second equivalent of the Grignard reagent was quickly consumed by the newly generated product, since the product has a more acidic proton than starting material. Although the metal-halogen exchange side reaction with Grignard was fast, it became non-competitive due to lack of the presence of the Grignard in the reaction mixture.

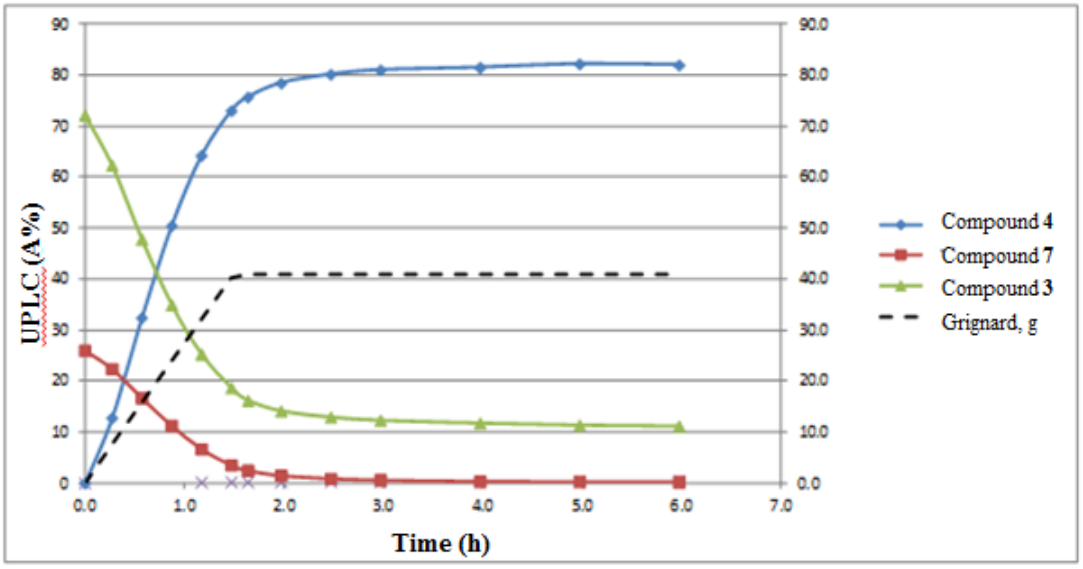

Figure 11. Kinetics Study of Grignard Reaction at 0 °C

It was later found that the addition mode in the Grignard reaction was less critical than the LiHMDS reaction. In the LiHMDS reaction, the base had to be added first to deprotonate **3**, before compound **7** was charged, to avoid the side reaction. Otherwise it would result in impurity formation. For the *i*-PrMgCl reaction, the base can be added before addition of **7**, in two portions before and after addition of **7**, or added directly to a mixture of **3** and **7**. The latter charging mode was selected because it greatly streamlined the operation on scale. Again, the fast kinetics provides the advantage for the Grignard reaction so the more convenient addition mode is feasible.

Process Development

1. Off-gassing Issue Associated with the Use of *i*-PrMgCl

With respect to selection of the Grignard reagent, we had initially selected *i*-PrMgCl because it is readily available at large scale. Since the consumption of *i*-PrMgCl produces propane gas, we needed to carefully consider the safety consequences. Our experiments showed that the dissipation of propane was dictated by the solubility of propane in THF, so slow dosing of Grignard reagent did not solve the issue. The propane gas accumulated in the reaction solvent and was released during the heating of the reaction mixture. A stage-wise heating protocol was defined to mitigate this off-gassing issue and this approach worked out well on pilot scale. It was determined, however, that this propane off-gassing would become unsustainable as the scale increased. Thus, a screening of different Grignard reagents was performed to identify a new Grignard without the off-gassing issue. The results of this effort are summarized in Table 3. While several Grignard reagents worked well, cyclohexylmagnesium chloride (CyMgCl) in THF was selected after taking into consideration the cost and the commercial availability.

Table 3. Grignard Base Screening Results

Entry	Grignard	Crude Yield	Product Purity	Product Assay
1	CyclohexylMgCl (THF)	86%	99.0%	100.0%
2	CyclohexylMgCl (2-MeTHF)	78%	99.5%	100.2%
3	CyclopentylMgCl (2-MeTHF)	86%	99.5%	99.5%
4	*t*-ButylMgCl (THF)	70%	99.2%	100%
5	*p*-TolylMgCl (THF)	81%	98.0%	93.3%
6	HexylMgCl (THF)	73%	99.7%	100.0%
7	IsopentylMgCl (Diethyl Ether)	74%	97.0%	84.8%
8	CyclohexylMgCl (Toluene/THF)	>100%	92.8%	85.2%
9	CyclohexylMgBr (THF)	>100%	97.1%	89.5%

2. Filtration Challenge

One of the major challenges with this process was the slow filtration of the product **4**. In the LiHMDS process, the reaction mixture was quenched with aqueous NH_4Cl and the product precipitated promptly during the aqueous quench. The filtration of the triphasic mixture (aqueous/organic/solid) was extremely slow, taking several days at 15 kg scale. The isolated solids were observed to have a fine needle morphology (Figure 12). Polymorph screening did not identify any addition solid forms.

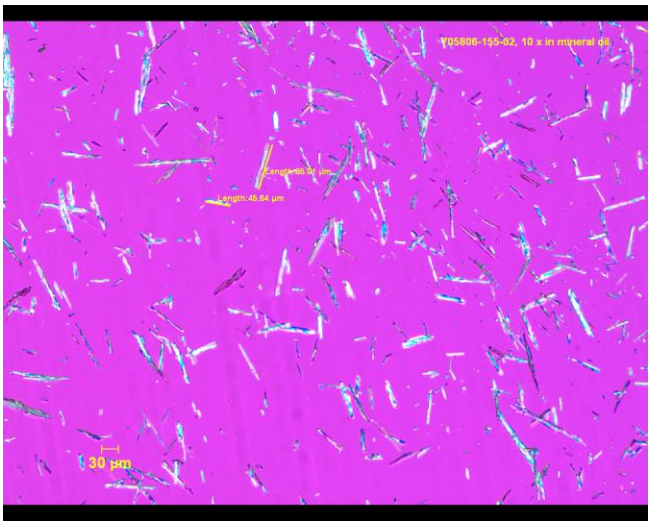

Figure 12. Typical Crystal Morphology Observed for 4

In addition, this compound has a very limited solubility in a broad spectrum of solvents. In most of solvents, the solubility is <1 mg/mL. Thus, the precipitation of the product was spontaneous upon the quench with water and development of a controlled crystallization process was not possible. In the enabling process, THF/toluene was used as reaction solvent and the filtration was very challenging. Considering that the THF is one of the better solvents for the product (albeit giving a solubility of 1.5 mg/mL at ambient temperature), it was decided to use pure THF as reaction solvent to relieve the over-saturation to some extent. Temperature cycling was also attempted to improve the aspect ratio and physical properties of the crystals, but this resulted in slower filtration due to particle attrition during the temperature cycling. Fortunately, the reaction mixture had acceptable stability at 60 °C, and reaction quench at 60 °C allowed for some control of the precipitation. The solvent change to pure THF and increased quench temperature improved the filtration rate four-fold, but the filtration was still slow.

The change of the base from LiHMDS to *i*-PrMgCl also required a change of the quenching protocol, because NH_4Cl generated poorly soluble magnesium salts, and these species resulted in problematic emulsions. Acetic acid, citric acid, hydrochloric acid, and tartaric acid were

evaluated for the quench and acetic acid was deemed to be optimal. A quench protocol with 0.75 M aqueous HOAc (8.5 vol) was developed and worked well at lab scale. However, when this process was scaled up, a bad emulsion was again observed. Experiments aiming at breaking up the emulsion using 10% aqueous NaCl or 10% aqueous Rochelle's salt successfully suppressed the emulsion, but resulted in precipitation of large quantity of inorganic salts in the product stream.

Due to the emulsions, the product was contaminated with insoluble magnesium salts, which resulted in difficult drying of the product, and water was determined to be detrimental to the subsequent Heck reaction. Aqueous washes of the filter cake, both displacement washes and slurry washes, were ineffective in reducing the inorganic content. The inorganic could only be reduced by reslurrying the crude product in a THF/aqueous acetic acid mixture. In the process of searching for a solution to this issue, a counter-intuitive approach was discovered. It was found that when the reaction mixture was quenched with acetic acid diluted with THF, in the absence of water, all of the inorganic materials remained in the mother liquor and the isolated product had a nearly 100 % assay. While the filtration was not complicated by the co-precipitation of the inorganics, this non-aqueous quench protocol also resulted in a much better filtration. It is believed that the solvent viscosity played some role in the filtration improvements. The THF-rich mother liquors are less viscous than the THF/water mixture used in the earlier processes.

3. Impurity Control Strategy

The isolation process effectively purges most of the process related impurities. Among all of the impurities, the des- bromo impurity **24** is the only impurity that progresses through the subsequent steps and has potential to impact drug substance quality. Two possible pathways

contribute to the formation of the des-bromo impurity (Scheme 10), both due to metal halogen exchange with Grignard bases.

Scheme 10. Formation of des-bromo impurity 24

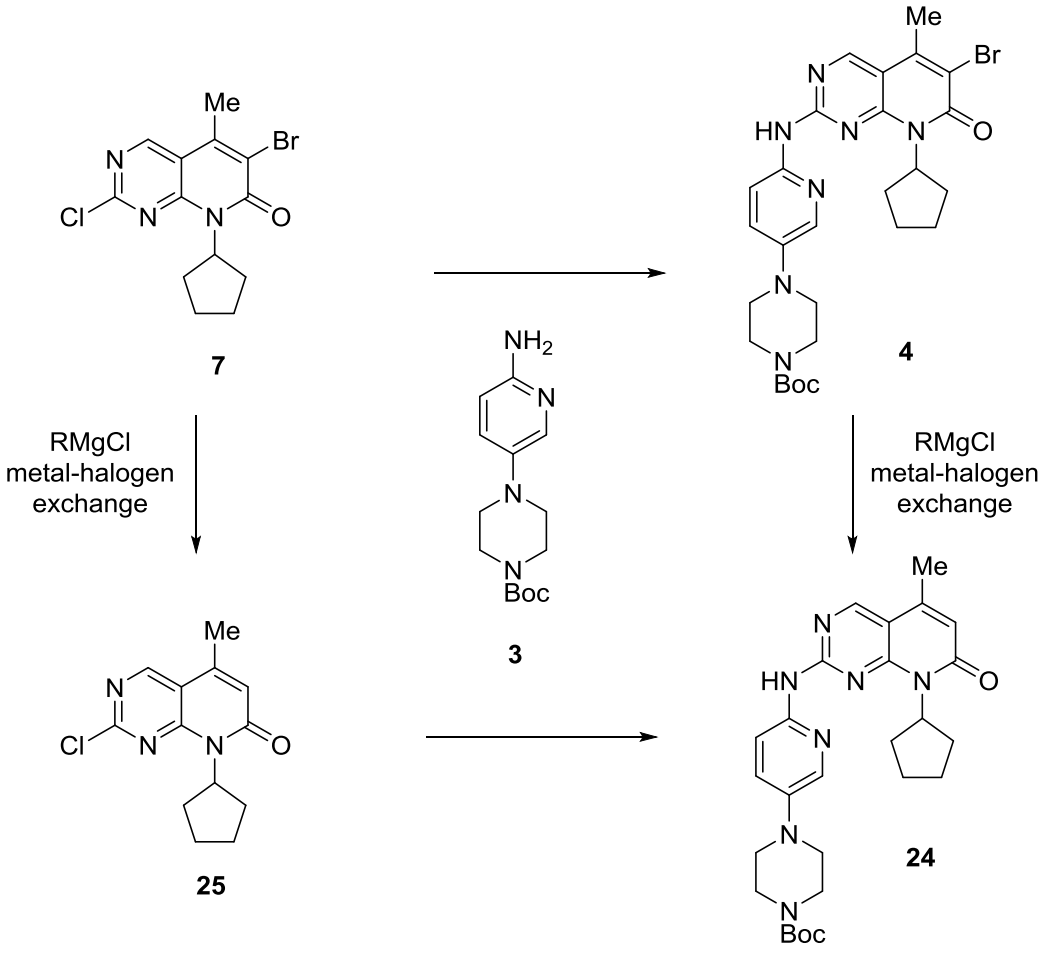

Multivariate design of experiment (DoE) studies were used to evaluate the impact of process parameters on the level of des-bromo impurity. Statistical analysis of reaction data showed that the reaction temperature has a significant impact on des-bromo level, which increases linearly as temperature increases. Significant interaction between the stoichiometry of **3** and cyclohexylmagnesium chloride stoichiometry was also detected. As shown in the contour plot below (Figure 13), elevated levels of des-bromo are observed at high reaction temperature, low

stoichiometry of **3** and high cyclohexylmagnesium chloride stoichiometry. In order to keep the des-bromo impurity at satisfactory level in the reaction, the reaction temperature range is defined as 0 to 30 °C.

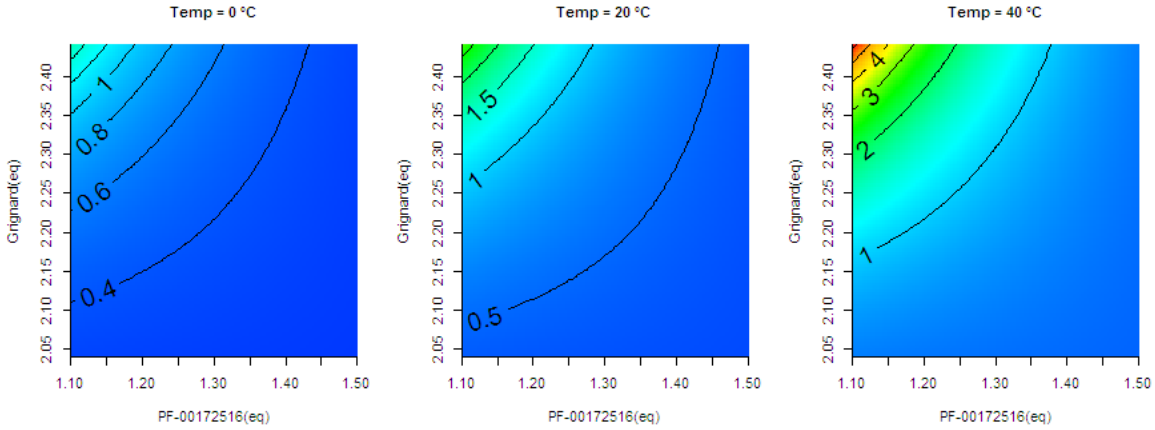

Figure 13. DoE Contour Plot of Des-Br (24) Formation Study

CONCLUSION

In summary, the S_NAr coupling between **3** and **7** was thoroughly studied. Through mechanistic and kinetics studies, the Grignard base was identified, which allowed for the reduction of the usage factor of **3.** The yield and the purity of the product were also enhanced. The initial off-gassing issue associated with the use of *i*-PrMgCl was resolved by switching to CyMgCl. The use of Grignard base also permitted charging the base into a mixture of the two starting materials, which simplified the process greatly. Finally, a non-aqueous quench was developed, which greatly improved the filtration rate. The CyMgCl process was successfully implemented in the commercial facility and was scaled up to prepare 130 kg of **4**.

EXPERIMENTAL SECTION

All reactions were performed under a nitrogen atmosphere. All reagents purchased from vendors were used as received. NMR data was collected using a Bruker AV III 600MHz spectrometer with TCI cryoprobe. HRMS data was obtained using a Thermo Orbitrap XL using Electrospray Ionization in positive mode. Reactions were monitored by reverse phase UPLC. UPLC conditions: BEH Shield RP18, 2.1 x 100 mm, 1.7 μm, 45 °C, flow 0.4 mL/min; λ = 295 nm, 3 μL injection volume; A: 0.1% formic acid in water; B: 0.1% formic acid in acetonitrile. Gradient 5% B to 95% B in 8 minutes, re-equilibrate to 5% B in 0.1 min. Diluent: 50:25:25 tetrahydrofuran: acetonitrile: purified water.

Preparation of tert-butyl 4-(6-(6-bromo-8-cyclopentyl-5-methyl-7-oxo-7,8-dihydropyrido[2,3-d]pyrimidin-2-ylamino)pyridin-3-yl)piperazine-1-carboxylate (4)

1. LiHMDS Process To a solution of **3** (42.7 kg, 153.2 mol) in tetrahydrofuran (THF, 341.7 kg) at 15 - 25 °C was added a solution of lithium hexamethyldisilazide in THF (100.4 kg, 138.6 mol). The resulting mixture was agitated for a minimum of 30 min. **7** (25.0 kg, 73 mol) was added portionwise. The resulting suspension was adjusted to 60 °C and stirred at 60 °C for 2 hours. Upon completion of the reaction, a solution of NH_4Cl (15.6 kg) in water (283 L) was added while maintaining the batch temperature <65 °C. The batch was then cooled to 20 °C. The aqueous layer was drained and the solids were collected by filtration. The filter cake was washed with acetone (2 × 100 L) and dried under vacuum at 65 °C to yield **4** (31.40 kg) as a yellow solid. HPLC purity 98.2%; yield 74%. **^{1}H NMR (600 MHz, THF-d_8):** δ 9.36 (s, 1H), 8.87 (s, 1H), 8.22 (d, *J* = 8.8 Hz, 1H), 8.04 (d, *J* = 2.9 Hz, 1H), 7.39 (dd, *J* = 8.8, 2.9 Hz, 1H), 6.10 (m, 1H), 3.55 (broad, 4H), 3.09 (broad, 4H), 2.60 (s, 3H), 2.30 (m, 2H), 2.09 (m, 2H), 1.85 (m, 2H), 1.66 (m, 2H), 1.46 (s, 9H); **^{13}C NMR (150 MHz, THF-d_8):** δ 159.5, 158.9, 157.7,

156.0, 155.0, 147.2, 144.62, 144.56, 138.0, 126.7, 117.6, 114.2, 108.4, 79.9, 55.5, 50.6, 44.7, 29.0, 28.7, 26.9, 18.1; **HRMS:** Calcd for $C_{27}H_{35}N_7O_3Br_1$ $(M+H)^+$: 584.19797, Found: 584.19811.

2. *i*-PrMgCl Process To a solution of **3** (58.2 kg, 209.2 mol) in THF (722.2 kg) at 15 – 25 °C was added a solution of iPrMgCl (93.4 kg, 19.5 wt/wt%, 177.0 mol) in THF. The resulting solution was agitated for a minimum of 30 min. 7 (55.14 kg, 160.9 mol) was added portionwise. The second portion of *i*-PrMgCl (93.4 kg, 177.0 mol) was added over at least 60 min. The batch was stirred at 20 °C for 90 min. and then adjusted to 60 °C slowly (at a rate of 0.5 °C/min). Upon reaction completion, a solution of glacial acetic acid (13.5 kg) in THF (183.6 kg) was added, followed by seeding with **4** (276 g). The resulting slurry was cooled to 20 °C, filtered, and the wet cake washed with acetone (331 L), water (331 L), and acetone (331 L). The crude product was dried under vacuum at 65 °C to yield **4** (79.4 kg) as yellow solid. HPLC purity 98.8%; yield 84.4%.

3. CyMgCl Process To a solution of **7** (35 g, 102.2 mmol) and **3** (37 g, 132.8 mmol) in THF (455 mL) at 15 – 25 °C was added a solution of cyclohexylmagnesium chloride (215 g, 224.8 mmol) while maintaining the batch temperature <25 °C. The batch was agitated at 20 °C for a minimum of 2 hours. Upon the completion of the reaction, the batch was quenched with a solution of acetic acid (8.6 g) in THF (105 mL). The resulting slurry was cooled to 20 °C, and the solids were collected by filtration. The crude product was dried under vacuum at 65 °C to yield **4** (50.8 g) as yellow solid. HPLC purity 99.5%; yield 85%; assay 100%.

AUTHOR INFORMATION

Corresponding Author

*Email: Shengquan.duan@pfizer.com

Present Addresses

† AbbVie, 1400 Sheridan Road, North Chicago, IL 60064

Notes

The authors declare no competing financial interest .

ACKNOWLEDGMENT

The authors wish to thank the Pfizer PDF operation staff and Pfizer PGS Ringaskiddy operation staff for their support during the clinical and commercial manufacturing. In addition, we would like to thank Yuriy Abramov for the computational work on the HOMO and pKa calculation. We are also grateful for the support from the Pfizer CRD process safety group.

REFERENCES

(1) (a) Nurse, P. *Cell* **2000**, 100, 71-78. (b) Malumbres, M.; Barbacid, M. *Trends Biochem. Sci.* **2005**, 30, 630-641. (c) Malumbres, M.; Harlow, E.; Hunt, T.; Hunter, T.; Lahti, J. M.; Manning, G.; et al. *Nat. Cell Biol.* **2009**, 11, 1275-1276. (d) Diaz-Moralli, S.; Tarrado-Castellarnau, M.; Miranda, A.; Cascante, M. *Pharm. Therapeutics* **2013**, 138, 255-271.

(2) (a) Bruyere, C.; Meijer, L. *Curr. Opinion in Cell Biol.* **2013**, *25*, 772-779. (b) Stone, A.; Sutherland, R. L.; Musgrove, E. A. *Crit. Rev. Oncogenesis* **2012**, *17*, 175-198. (c) Wesierka-Gadek, J.; Maurer, M.; Zulehner, N.; Komina, O. *J. Cell Physiol*. **2011**, *226*, 341-349. (d) Shapiro, G. *J. Clin. Oncol*. **2006**, *24*, 1770-1783.

(3) Toogood, P. L.; Harvey, P. J.; Repine, J. T.; Sheehan, D. J.; VanderWel, S. N.; Zhou, H.; Keller, P. R.; McNamara, D. J.; Sherry, D.; Zhu, T.; Brodfuehrer, J.; Choi, C.; Barvian, M. R.; Fry, D.W. *J. Med. Chem.* **2005**, 48, 2388.

(4) Erdman, D. T.; Flamme, C. M.; Nelson, J. D. Synthesis of 2-(pyridine-2-ylamino)-pyrido[2,3-d]pyrimidin-7-ones, PCT Int. Appl. WO 032157 A2, **2008**

(5) 1.2% regioisomer was observed without additives; 0.3-0.6% regioisomer was observed with LiOTf as additive. SMB (simulated moving bed) purification was required to remove this impurity at above 1.0% level, in order to meet the API specifications.

(6) Toogood, P. L.; Ide, N. D. Palbociclib (Ibrance): The First-in-Class CDK4/6 Inhibitor for Breast Cancer. In *Innovative Drug Synthesis*; John Wiley and Sons, Inc. **2016**, pp 167-195.

(7) Kienle, M.; Dubbaka, S. R.; Brade, K.; Knochel, P. Eur. *J. Org. Chem.* **2007**, *20*, 4166-4176.

(8) Marco-Contelles, J.; Pérez-Mayoral, E.; Samadi, A.; do Carmo Carreiras, M.; Soriano, E. *Chem. Rev.* **2009,** *109*, 2652-2671.

(9) Kadnikov, D.V.; Larock, R. C. *J. Org. Chem.* **2004,** *69*, 6772-6780.

(10) Sai, K. K. S.; Gilbert, T. M.; Klumpp, D. A. *J. Org. Chem.* **2007,** *72*, 9761-9764.

(11) Maloney, M. T.; Jones, B. P.; Olivier, M. A.; Magano, J.; Wang, K.; Ide, N. D.; Palm, A. S.; Bill, D. R.; Leeman, K. R.; Sutherland, K.; Draper, J.; Daly, A. M.; Keane, J.; Lynch, D.; O'Brien, M.; and Tuohy, J. *Org. Process Res. Dev.* **2016**, xxxx – xxxx

(12) Chekal, B. P.; Ewers, J.; Guinness, S. M.; Ide, N. D.; Leeman, K. R.; Post, R. J.; Rane, A. M.; Sutherland, K.; Wang, K.; Webster, M.; Withbroe, G. J.; Draper, J.; Lynch, D.; McAucliffe, M.; and Keane, J. *Org. Process Res. Dev.* **2016**, xxxx-xxxx

(13) A few impurities, including the product from pyridine nitrogen attack, and two possible dimeric impurities, were observed in this reaction.

(14) (a) Volovenko, Y. M.; Blyumin, E.V. *Tetrahedron Lett.* **2000,** *56,* 5185-5191. (b) Maloney, K. M.; Kuethe , J. T.; Linn, K. *Org. Lett.* **2011,** *13,* 102-105. (c) Wei, X.; Shu, C.; Haddad, N.; Zeng, X.; Patel, N. D.; Tan, Z.; Liu, J.; Lee, H.; Shen, S.; Campbell, S.; Varsolona, R. J.; Busacca, C. A.; Hossain, A.; Yee, N. K.; Senanayake, C. H. *Org. Lett.* **2013,** *15*, 1016-1019.

(15) VanderWel, S. N.; Harvey, P. J.; McNamara, D. J.; Repine, J. T.; Keller, P. R.; Quin, J., III; Booth, R. J.; Elliott, W. R.; Dobrusin, E. M.; Fry, D. W.; Toogood, P. L. *J. Med. Chem.* **2005**, 48, 2371−2387.

(16) Note compound **11** is a potential sensitizer.

(17) (a) Surry, D. S.; Buchwald, S. L. *Angew. Chem. Int. Ed.* **2008**, *47*, 6338- 6361 and the references therein. (b) Reddy, Ch. V.; Kingston, J. V.; Verkade, J. G. *J. Org. Chem.*, **2008**, *73*, 3047-3062.

(18) Kowalski, P.; Korchowiec, J. *J. Mol. Struct. (Theochem)*, **1993**, *288*, 119-131.

(19) Shen, Z.; Hong, Y.; He, X.; Mo, W.; Hu, B.; Sun, N.; Hu, X. *Org. Lett.* **2010,** *12*, 552-555.

(20) Shi, Y.-J.; Humphrey, G.; Maligres, P. E.; Reamer, R.A.; Williams, J. M. *Adv. Synth.Catal.* **2006**, *348*, 309-312

(21) Sieser, J. E., Singer, R. A. et al. *Org. Process Res. Dev.* **2011,** *15(6),* 1328-1335

(22) Senanayake, C. H., Hong, Y. et al. *Tetrahedron Lett.* **1999,** *40,* 6875 – 6879

(23) (a) Chapman, A.W. *J. Chem. Soc.* **1927**, 1743 (b) Kimura, M. *J. Chem. Soc. Perkin Trans. II* **1987**, 205-209 (c) Suttle, N. A.; Williams, A. *J. Chem. Soc. Perkin Trans. II* **1983**, 1369-1372

(24) Ryabova, S. Y.; Alekseeva, L. M.; Listiza, E. A.; Shashkov, A. S.; Chernyshev, V. V.; Tichomirova, G. B.; Goyzman, M. S.; Granik, V. G. *Russ. Chem. Bull., Int. Ed.*, **2001**, *50,* 1449-1456.